Climatic Change (2007) 81:233–247
DOI 10.1007/s10584-006-9229-9

Summertime inter-annual temperature variability in an ensemble of regional model simulations: analysis of the surface energy budget

G. Lenderink · A. van Ulden · B. van den Hurk · E. van Meijgaard

Received: 15 February 2005 / Accepted: 17 October 2006 / Published online: 17 March 2007

Abstract The inter-annual variability in monthly mean summer temperatures derived from nine different regional climate model (RCM) integrations is investigated for both the control climate (1961–1990) and a future climate (2071–2100) based on A2 emissions. All regional model integrations, carried out in the PRUDENCE project, use the same boundaries of the HadAM3H global atmospheric model. Compared to the CRU TS 2.0 observational data set most RCMs (but not all) overpredict the temperature variability significantly in their control simulation. The behaviour of the different regional climate models is analysed in terms of the surface energy budget, and the contributions of the different terms in the surface energy budget to the temperature variability are estimated. This analysis shows a clear relation in the model ensemble between temperature variability and the combined effects of downward long wave, net short wave radiation and evaporation (defined as F). However, it appears that the overestimation of the temperature variability has no unique cause. The effect of short-wave radiation dominates in some RCMs, whereas in others the effect of evaporation dominates. In all models the temperature variability and F increase when imposing future climate boundary conditions, with particularly high values in central Europe.

1 Introduction

The summer of 2003 has been excessively warm in large parts of Europe with monthly mean temperatures in central Europe exceeding the previous observed maximum by 2° or more (Schär et al. 2004; Luterbacher et al. 2004; Beniston and Diaz 2004). Schär et al. (2004) estimated the chance that these high temperatures would occur under

G. Lenderink (✉) · A. van Ulden · B. van den Hurk · E. van Meijgaard
Royal Netherlands Meteorological Institute, Postbus 201, De Bilt 3730 AE, The Netherlands
e-mail: lenderin@knmi.nl

present-day climate conditions to be extremely low. They presented results of a regional climate model (RCM) integration, which predict that the mean temperature as well as its inter-annual variability will increase compared to the present-day conditions. They concluded that an increase of the variability of the summertime temperatures could drastically increase the probability of extremely warm summer events, and hypothesize that the 2003 summer conditions might be a manifestation of this effect.

Temperature variability is determined by combined effects of the large-scale atmospheric circulation and small-scale physical processes, like long and short wave radiation, boundary-layer turbulence and soil processes determining latent and sensible heat fluxes. In atmospheric models, these smaller scale physical processes are parameterized by cloud, radiation, soil and turbulence schemes. As such, these parameterization schemes exert a strong control on the temperature variability. For example, a soil scheme that is sensitive to drying may lead to high temperature in summer (Seneviratne et al. 2002). Although there is ample literature about these processes in individual models (Räisänen et al. 2004; Vidale et al. 2003; Giorgi et al. 2004), no comprehensive summary of how they operate in a suite of models exists to date.

In the European project PRUDENCE (Prediction of Regional scenarios and Uncertainties for Defining EuropeaN Climate change and Effects; Christensen and Christensen 2007) nine different RCMs are used to simulate both present-day climate (1961–1990) and future climate (2071–2100). These simulations are all driven by the same boundaries, which approximately enforce the same statistics of the large scale dynamics in the model domain (Van Ulden et al. 2007). Therefore, this ensemble provides an ideal testbed to analyse the impact of the differences in the physics parameterizations on the model behavior, and in particular on the simulated temperature variability. As a first step in this process, we consider in this study differences in the simulated surface energy budget and relate these to the differences in summertime temperature variability. In Vidale et al. (2007) the relation between soil moisture and temperature variability is studied in the same PRUDENCE model ensemble.

2 Temperature variability compared to observations

We used nine different RCMs driven by HadAM3H boundaries and the A2 emission scenario. Data of two time slices are considered: 1961–1990 (representing the present-day climate) and 2071–2100 (representing the future climate). The RCMs are: HIRHAM, CHRM, CLM, HadRM3H, RegCM, RACMO2, REMO, RCAO, PROMES. Details on these RCMs and the experimental setup of the integrations can be found in Jacob et al. (2007) and Christensen and Christensen (2007) in this issue. From the available RCMs integrations monthly mean output was obtained from the PRUDENCE data base (http://prudence.dmi.dk). The temperature time series of the future climate integration (2071–2100) are detrended using the trend over that period in HadAM3H over the northern hemisphere (2°C over 30 years). This detrending has a small impact (compared to the climate change signal) on the computed values for the temperature variability.

The RCM output is compared to the Climate Research Unit (CRU) TS 2.0 observational time series (New et al. 2000) of monthly means (period 1961–1990) on a regular 0.5 × 0.5 degree lat-lon grid (see also Jacob et al. 2007). As a measure of the variability the inter-quartile range (IQR) (between the 25% and 75% quantiles) is considered for each summer month. For the CRU observations results are shown in Fig. 1. In general, the temperature variability is largest in June, and smallest in August, with the exception of central Germany and France where the temperature variability is largest in July. For most areas the inter-quartile range is about 1.5 − 2.5°C for all summer months, with the lowest values for August. Figure 1 also shows four different areas used for further analysis: Southern France (SFRA), Germany (GER), Spain (SPA) and Southeastern Europe (SEU). For the RCMs and the driving HadAM3H simulation the difference with the CRU observations is shown in Fig. 2.

The HadAM3H results (Fig. 2 left panels on top) show reasonably small deviations in IQR from the CRU observations in June (except in Spain). In August, and to a lesser extent in July, the deviations are larger, typically a 1-2°C overestimation in large parts of central and eastern Europe.

The outcome of the regional models show a large spread around the HadAM3H results; some models are clearly closer to the observations while others are deviating more. The temperature variability in RACMO2, CLM, CHRM, and REMO is (rather) close to the observations, but the remaining 5 models overpredict the IQR in central (including France) and southeastern Europe, up to more than 2 degrees (100%) in HadRM3H, PROMES and RegCM. For this area some models show a clear increase in variability during the course of the summer (HadRM3H, HIRHAM, and to a lesser extend RCAO and REMO), suggesting that progressive soil drying during summer plays a role. In particular striking is the large increase in variability from the HadAM3H global simulation to the regional HadRM3H simulation, considering that both models essentially share the same model physics. Further analysis (not shown) revealed that most models overestimate the temperatures in the high tail of the distribution, with the exception of PROMES and CLM which underestimate temperatures in the low tail.

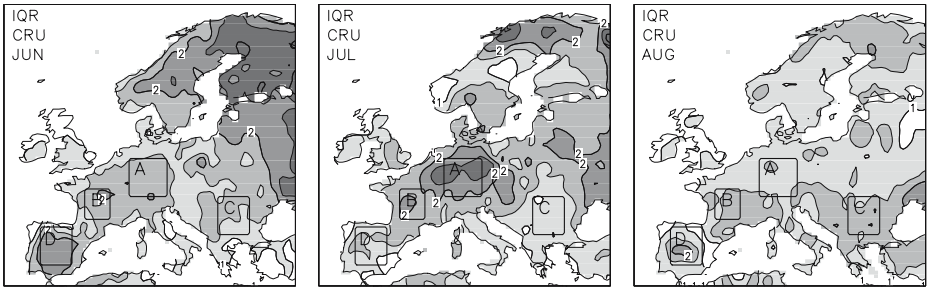

Fig. 1 Interquartile range (*IQR*) of the monthly mean temperature in the CRU observations for June, July, and August. Shading interval 0.5°C, starting at 1°CL. Also shown are four different areas: *GER* (**A**), *SFRA* (**B**), *SEU* (**C**), and *SPA* (**D**)

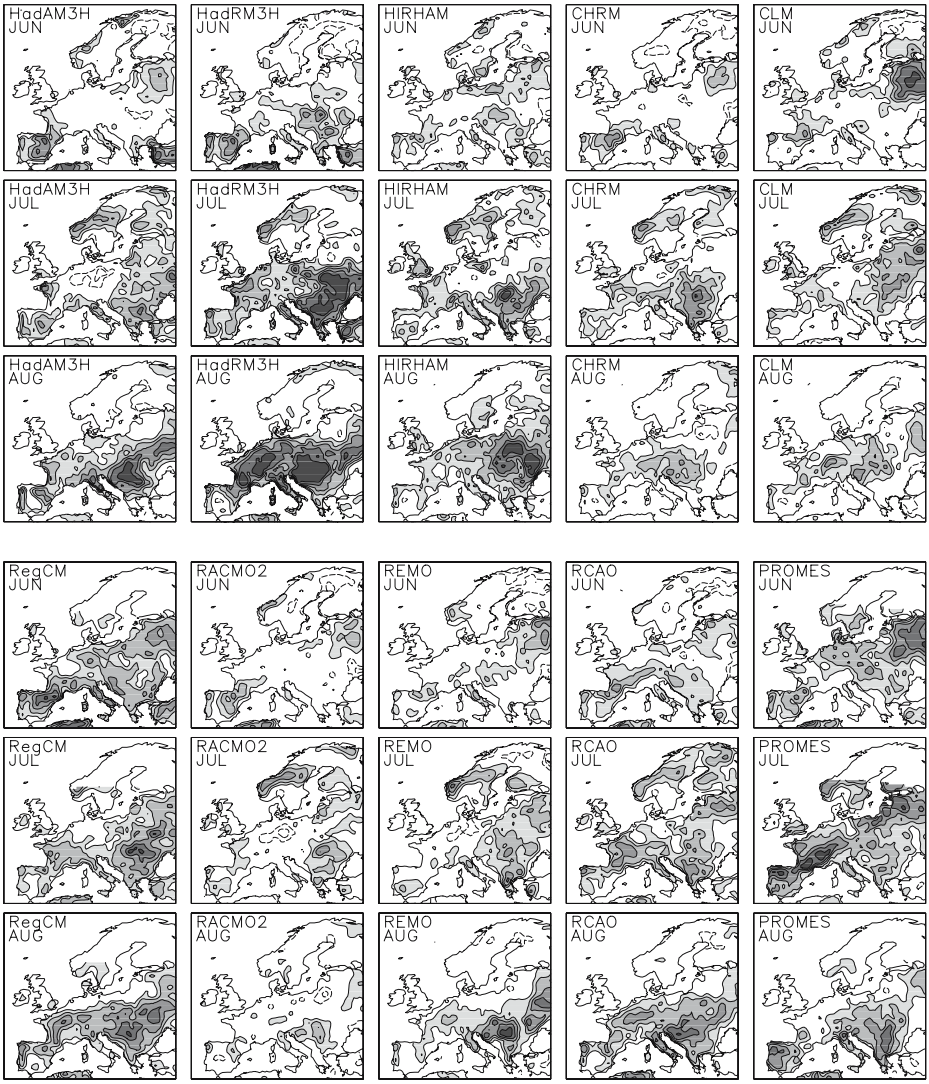

Fig. 2 IQR of the monthly mean temperature in HadAM3H and the RCM ensemble. Shown are anomalies to the CRU observations. *Shading* starts at 0.5°C with steps of 0.5°C. *Dashed contours* denote negative values below -0.5°C

3 Evaporation and radiation

3.1 Mean fluxes

To illustrate the typical differences across Europe, we show mean fluxes of evaporation and net short-wave radiation at the surface in Fig. 3 for two areas, GER (relatively wet and cloudy) and SPA (dry and sunny). Results for SFRA and SEU (not shown) are in between. Evaporation is used here for the total evaporation

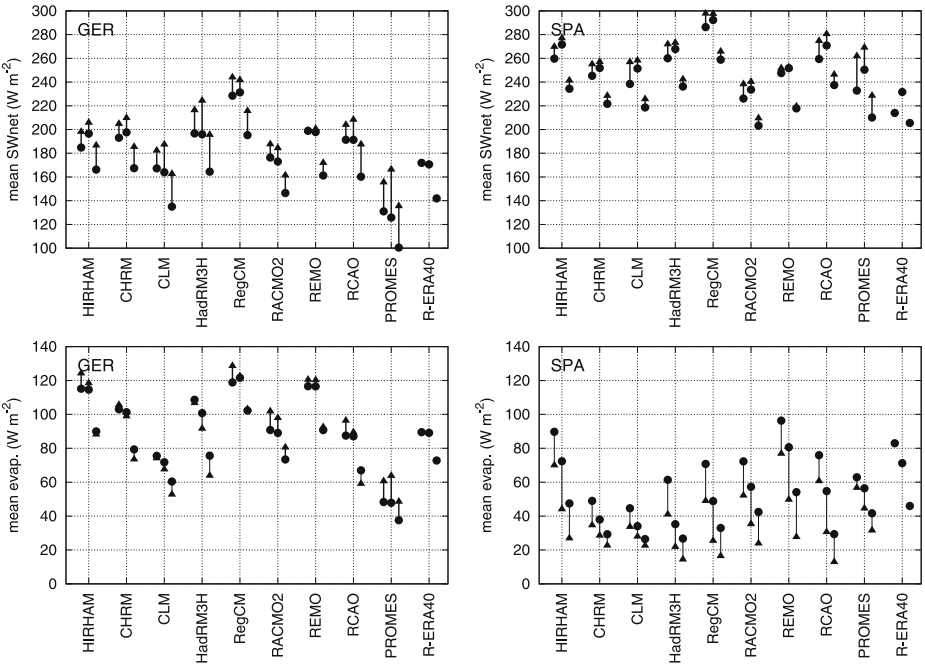

Fig. 3 Mean net short-wave radiation and evaporation for GER and SPA. For each RCM results for June, July and August (*three consecutive symbols/lines*) are shown. *Solid dots* (*triangles*) are results for the control (*future*) integration, with a thick (*thin*) l*ine* denoting *increase* (*decrease*) from control to future simulation

from the surface, including transpiration from the vegetation, which is (in hydrological sciences) commonly denoted as evapotranspiration. For both evaporation and short wave radiation, the spread in the model ensemble is considerable. We note that, in general, there appears to be a (small) compensation between shortwave radiation and evaporation with models with high surface radiation tending to have large evaporation rates, and vice-versa. This might partly be a consequence of the way models are tuned, since high (low) surface insolation, leading to high surface temperatures, may be compensated by high (low) evaporation rates. Conversely, cloud radiative properties and thereby surface insolation may also be adjusted to compensate for anomalous evaporation rates. While such tuning may be successful for the simulation of the mean temperature, it may also have important implications for the simulated temperature variability. For example, the low mean value of radiation in PROMES suggests a strong cloud-radiation control, which also appears to impact on the simulated temperature variability in that model (as will be shown in the next sections).

Net short wave fluxes in the model ensemble are about 60 Wm^{-2} lower and evaporation rates are about 40 Wm^{-2} higher in GER than in SPA. Evaporation is determined by the drying capacity of the atmosphere (often measured by the potential evaporation) restricted by limitations imposed by the dryness of the soil. Potential evaporation is strongly linked to the amount of net short wave radiation at the surface and the water vapor deficit between the surface and the atmosphere, both

of which are larger in SPA than in GER, and therefore soil water depletion plays a larger role in SPA than in GER. The reduction of evaporation during summer in SPA also is caused by the progressive drying of the soil.

3.2 Method of analysing variability

To analyse the relation between surface fluxes and temperature, we define an "average" difference in the surface flux that is related to the temperature variability as follows. First, for each area and each summer month, we sorted the 30-year time series of the monthly-mean, area-mean temperature. Figure 4 shows a quantile plot of such sorted temperatures for August in GER. At the same time we ordered the surface energy flux using the temperature as sorting criterion. For the same month and area, the co-sorted data for short-wave radiation and evaporation is plotted in Fig. 4. (Note that the position on the *x*-axis identifies the same month out of the 30-year period in each plot.) For short wave radiation a significant amount of scatter is obvious. However there is also a clear trend with, as expected, the highest amounts of short wave radiation occurring in the warmest months out of the 30-year period. Then, a straight line is fitted through the data using a least squares fit, and the difference between the value of the fit at the 100% quantile with the value at the 0% quantile is defined as ΔSWnet. Similar definitions are used for the other terms in the surface energy budget; e.g. Δevap for evaporation. The same definition is

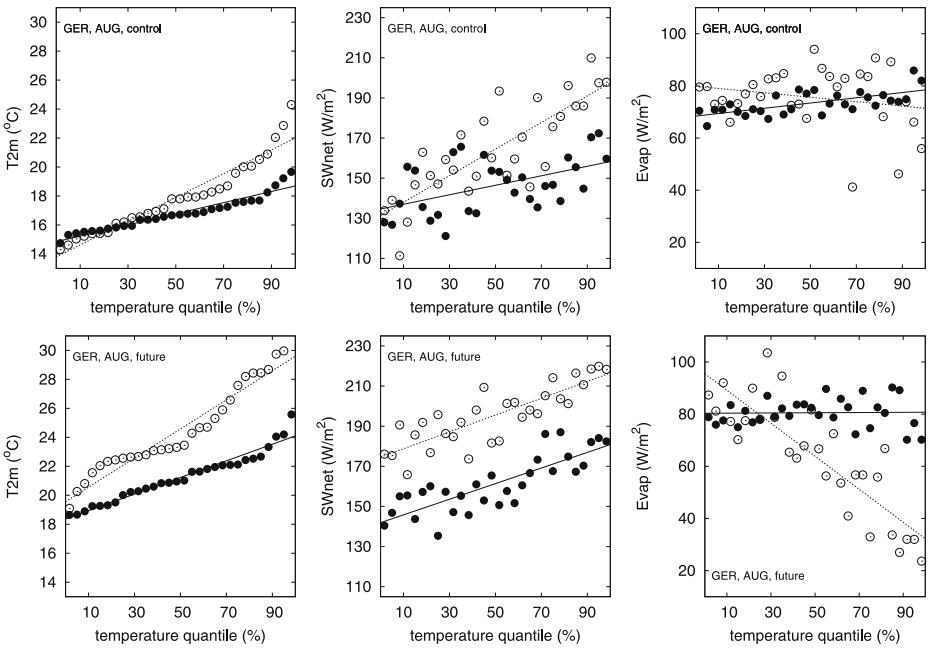

Fig. 4 Scatter plots of area averaged (for area GER in August) mean temperatures, net short-wave radiation and evaporation at the surface against temperature quantile (*see text*). Results are shown for RACMO2 (*solid dots*) and HadRM3H (*open circles*), both for the control (*upper panels*) and the future (*lower panels*) integration

also used for temperature variability, computing Δt2m from a fit through the sorted temperature data; Δt2m is about 3.3 times the standard deviation in all RCMs for each area and each summer month.

Figure 4 illustrates the typical differences in the model ensemble by showing results for RACMO2 and HadRM3H. For the control simulation ΔSWnet in HadRM3H is much larger than in RACMO2, and therefore short wave radiation contributes stronger to the temperature variability in HadRM3H than in RACMO2. For evaporation the slope of the fit for RACMO2 is positive – signifying higher evaporation rates in warm August months than in cold August months – and therefore evaporation acts to reduce the temperature variability. In HadRM3H the slope is negative, and evaporation therefore contributes to the temperature variability. The future integration shows an increase in mean short-wave radiation in both models, but ΔSWnet increases in RACMO2 and decreases in HadRM3H. Evaporation shows a very strong response in HadRM3H, with almost no evaporation in the warm months, and almost no response in RACMO2. Thus, in RACMO2 variability in short wave radiation contributes to the increased temperature variability, while in HadRM3H the contribution of the change in evaporation is dominant.

3.3 The control period

We applied this methodology first to the surface fluxes of net short wave radiation, downward long wave radiation, and evaporation. Figures 5, 6, 7 and 8 show Δt2m,

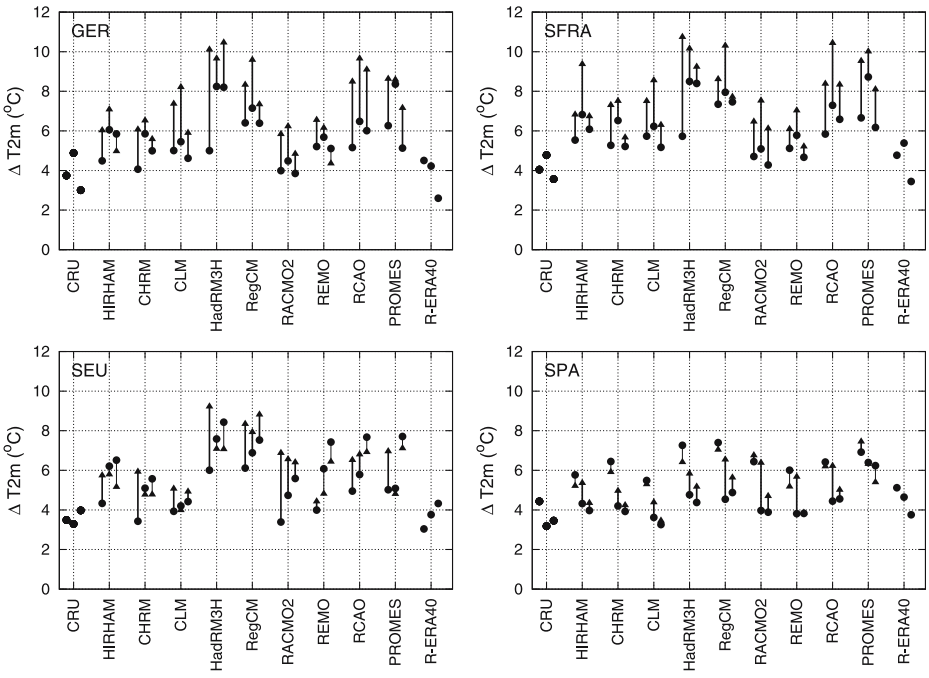

Fig. 5 Panels of Δt2m for GER, SFRA, SEU, and SPA for each RCM integration, and the CRU observation (*lines and symbols* as Fig. 3)

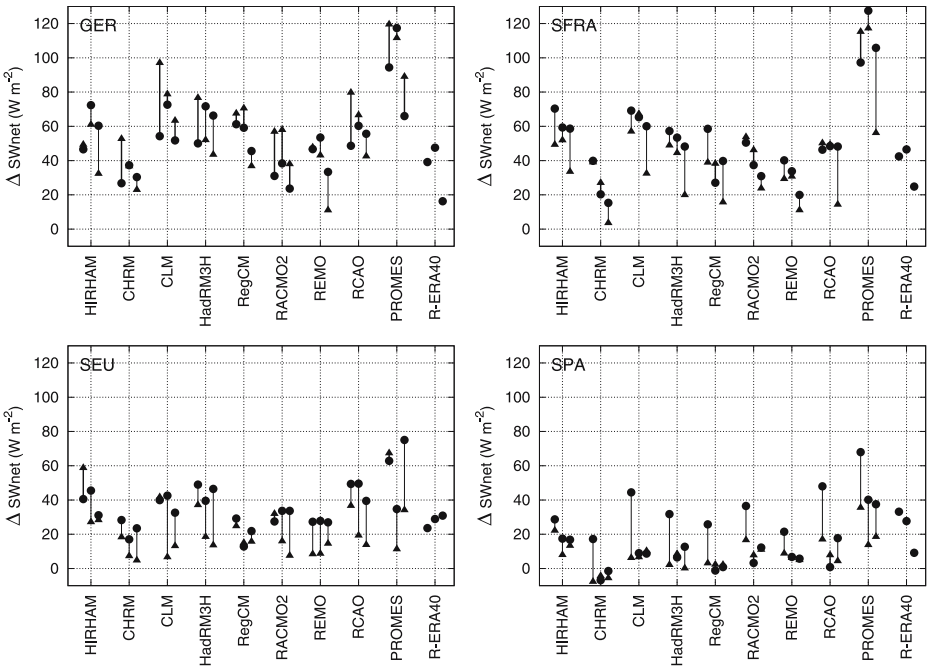

Fig. 6 As Fig. 5, but now for ΔSWnet (no observations)

ΔSWnet, Δevap, and ΔLWdown for each summer month and each area defined, both for the control simulation as for the future simulation. For evaporation we plotted-Δevap, so that positive plotted values correspond to a positive contribution to the temperature variability.

There are large differences in simulated short-wave radiation among the different RCMs: in particular for SFRA and GER, ΔSWnet ranges from 20 to 100 Wm^{-2}. The high temperature variability in PROMES as shown in Fig. 5 appears to be related to the large variability in short wave radiation (Fig. 6). Conversely, CHRM and RACMO2 have rather low values of ΔSWnet. All models show a decrease in ΔSWnet from GER and SFRA to SEU and SPA, showing that the influence of clouds on the radiative budget is larger in central Europe than in southern Europe.

Figure 7 shows results for evaporation. For the relative moist conditions in GER the majority of the RCMs reveal no signs of reduced evaporation by soil moisture depletion, which is reflected by the positive values of Δevap. Thus evaporation acts to reduce temperature variability. Exceptions are August in HadRM3H and all summer months in CLM. The dryer conditions in SFRA lead to a much larger model spread, with some models sustaining high evaporation in the warm months (PROMES, REMO and RACMO2) relative to the evaporation in cold months, whereas others clearly show the influence of the soil moisture depletion in warm months on evaporation. In SEU all models (except PROMES) again agree in predicting negative values of Δevap. Most models produce rather large negative values, therefore acting to enhance temperature variability significantly. Thus, SEU is characterized by a significant soil moisture control in all RCMs. Going further into

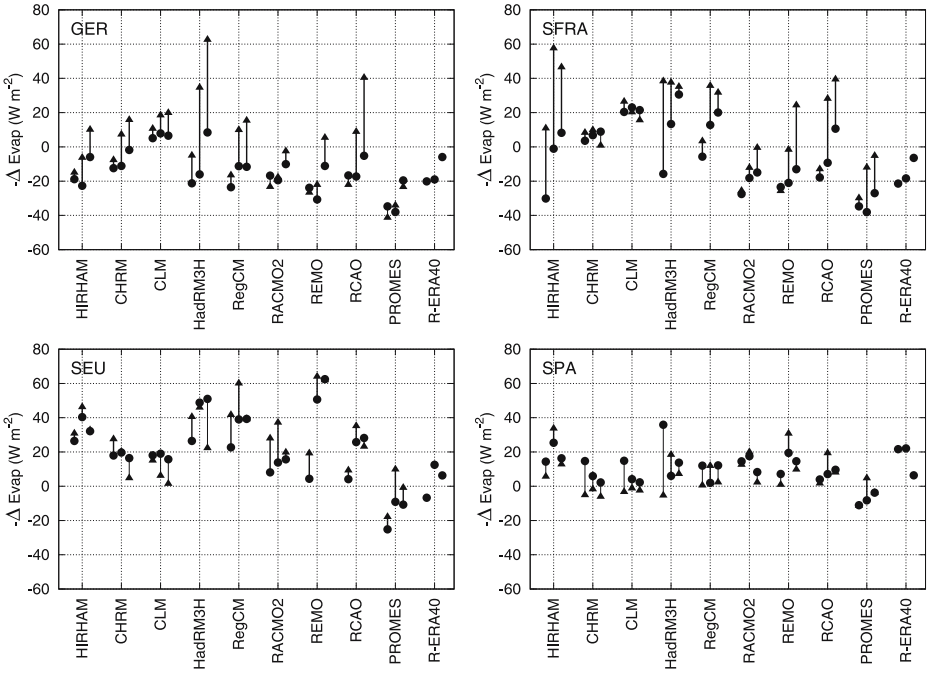

Fig. 7 As Fig. 5, but now for -Δevap (*no observations*)

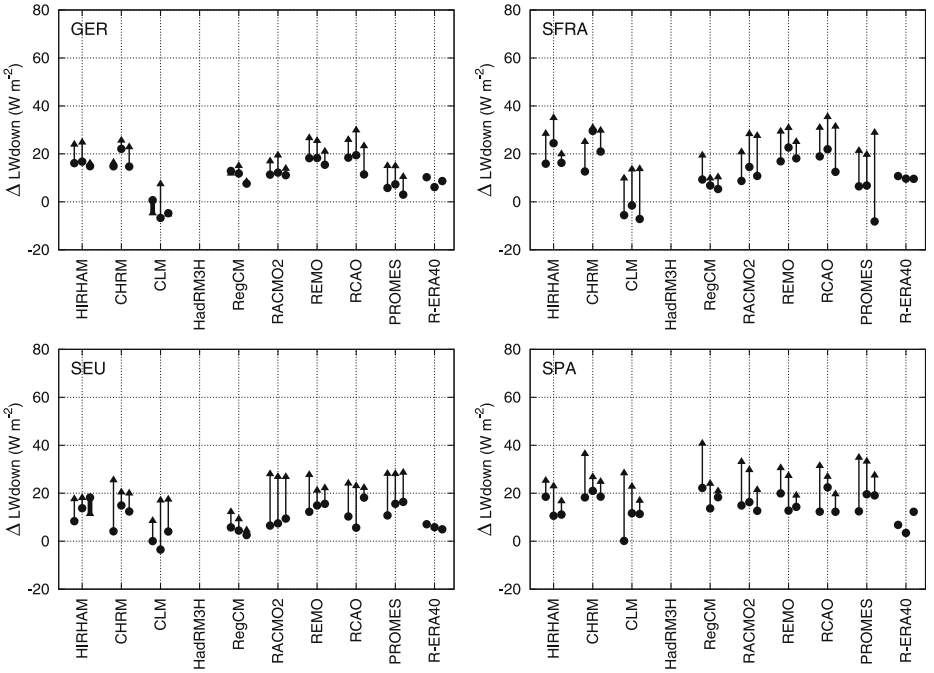

Fig. 8 As Fig. 5, but now for ΔLWdown (*no observations*)

the dry limit, all RCMs show smaller (and negative) values of Δevap in SPA. In the limit of a completely dry soil both mean evaporation and Δevap necessarily approach zero since there is no more moisture available for evaporation. In HadRM3H, for example, this explains the increase in Δevap from -38 Wm^{-2} in June, when the soil is not completely dried out yet, to close to zero in August.

The models results are rather consistent with respect to the downward long wave radiation (positive downward) as shown in Fig. 8, with values of ΔLWdown of 10–20 Wm^{-2} for the majority of the models (HadRM3H not reported). Two models are outliers with values of ΔLWdown close to zero (PROMES and CLM), which is most likely caused by the strong cloud-radiation control in these models. Clouds act to increase the downward long wave radiation since they increase the effective radiative temperature of the atmosphere. Since warm months are associated with small amounts of clouds (and vice-versa), clouds cause a reduction of ΔLWdown. The hypothesis of a strong cloud-radiation control is also consistent with the results for short wave radiation for these models.

3.4 The climate response

Figures 5, 6, 7 and 8 also show the results for the future climate runs (triangles). In general, the temperature variability, as measured by Δt2m, increases for each summer months and each area. For GER and SFRA the increase in temperature variability is considerable in most models, but for SEU and SPA the increase is not as clear. For SEU the RCMs disagree, with some models predicting (almost) no increase (e.g. HIRHAM and CLM) and others predicting a large increase (e.g. RACMO2). In SPA the agreement between the different RCMs is larger, with most models predicting almost no increase in June and a small increase in July and August.

For SFRA and SEU most RCMs display a decrease of ΔSWnet from the control climate integration to the future integration. In GER the models diverge with some models predicting an increase (e.g. CLM and RACMO2) while others predicting a decrease (e.g. HIRHAM and RCAO). In SPA ΔSWnet approaches zero, which is an manifestation of the fact that clouds are virtually absent (in the sense that they influence the radiative budget) in SPA even in "cold" months. The vast majority of the RCMs predicts an increase of the contribution of evaporation to the temperature variability in GER and SFRA, but the magnitude varies considerably with values of the change in Δevap between close to zero and -40 Wm^{-2}. CLM has almost no response, and also the response in RACMO2 and PROMES is relatively small. HIRHAM, RCAO and HadRM3H have relatively large responses. In particular, the large response in June in HadRM3H in SFRA shows that the drying out of the soil start to limit evaporation already early in summer. It is worthwhile noting that this corresponds to the large increase in temperature variability for June in HadRM3H. For SPA and SEU the response of Δevap is in general small. For SPA this mainly reflects that the models are close to their wilting points, and have very low mean evaporation between 20 and 60 Wm^{-2} (Fig. 3). Finally, for each area and each summer month ΔLWdown increases (Fig. 8). The increase is largest for southern Europe (areas SPA and SEU). There is a large agreement between the different RCMs, except PROMES which shows a significantly larger response for SFRA, and CLM which (still) shows very low values for GER compared to the other models.

4 Surface energy budget and temperature variability

In order to be able to tie differences in surface fluxes to differences in the temperature variability, we focus on the surface energy budget which for this purpose we write as:

$$LW_{up} + H + G = LW_{down} + SW_{net} - LE \equiv F,$$

with H sensible heat flux, LE the latent heat flux (evaporation), and G the soil heat flux, and LW_{down}, LW_{up} and SW_{net} the fluxes of downward long-wave, upward long-wave and net short-wave radiation, respectively. In this equation, we deliberately separated the terms which are strongly and physically dependent on the surface temperature on the left hand side from the other terms which have a weaker dependency on the surface temperature or are constrained by other quantities (e.g. soil moisture or atmospheric humidity in the case of evaporation). The sum of the terms on the right-hand side defines F. Obviously this separation is not a very strict

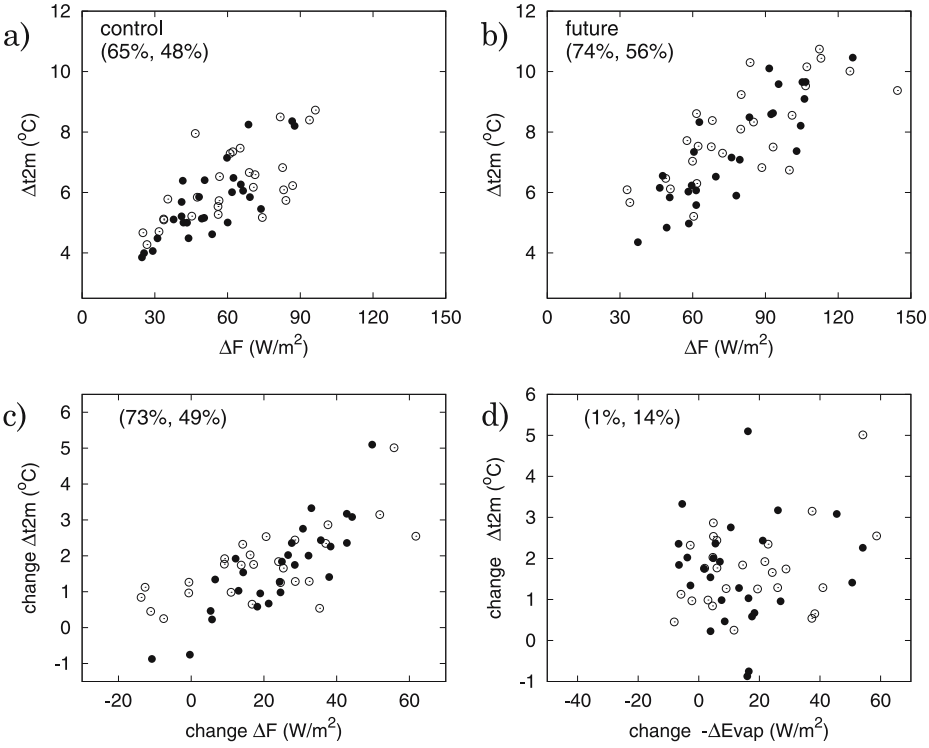

Fig. 9 Scatter plot of Δt2m against ΔF=ΔSWnet− ΔEvap+ΔLWdown for the **a** control integration, and the **b** future integration. Change in temperature variability (A2-Control) against **c** change in ΔF and **d** change in ΔEvap. Results are shown for all models and each summer month for *SFRA* (*open circles*) and *GER* (*dots*). For HadRM3H we set ΔLWdown to the mean of the model ensemble. Between parentheses is the explained variance (%) for (*GER,SFRA*)

separation, but if for the moment we accept it, we expect a scaling of the surface temperature variability on the variability in F. This follows from writing the equation as $R(T_s) = F$, with $R(T_s)$ a function of the surface temperature determined by the terms on the left-hand side, linearizing this function R around the 30-year mean temperature, and assuming that F is independent on the surface temperature.

Figure 9 shows the relation between temperature variability Δt2m and ΔF (combining ΔSWnet, ΔEvap and ΔLWdown) for the areas SFRA and GER. In the model ensemble, there is a clear relation between surface forcing ΔF and the temperature variability. This holds for both the control and the future climate simulation separately, but also for the changes between control and future simulation. The explained variance is between 50–70%, with in general the highest values for GER. For both areas the surface forcing ΔF increase from the control to the future simulation. For GER the slope of a linear fit between surface forcing and temperature variability is almost constant, ranging between 0.06 K $(\mathrm{Wm}^{-2})^{-1}$ for both control and future simulation and 0.075 K $(\mathrm{Wm}^{-2})^{-1}$ for the climate response. The slope may be used to estimate the contribution of the individual components, such as Δevap and ΔSWnet, to the temperature response. Figure 9d shows that the change in Δevap does not correlate well with the change in temperature variability. The same applies to the change in ΔSWnet (not shown). However, the sum of short wave radiation and evaporation correlates much better. The results are close to Fig. 9c, shifted by 10–20 Wm^{-2} to the left, and with slightly more scatter. Apparently, those models that have a weak response in evaporation are also characterized by a strong response the short wave radiation and vice-versa (as is e.g. illustrated for HadRM3H and RACMO2 in Fig. 4). Further interpretation of F and a discussion of other terms in the energy budget can be found in Lenderink et al. (2006)

5 Discussion

5.1 Circulation, land-sea temperature contrast and the surface energy budget

The analysis described above gives insight in the contributions of different terms in the surface energy budget to the temperature variability. A further analysis (results not shown) revealed that a large part of the surface fluxes are (highly) correlated with the circulation. For example, the short wave radiation is highly correlated with the circulation with westerly flows bringing cloudy and easterly flows bringing cloud-free conditions. For evaporation this relation is not so clear. Easterly winds bring dry, warm, and sunny conditions thereby enhancing evaporation, but prolonged easterly winds may cause a drying out of the soil that reduces evaporation. The advection of warm air from the continent causes an increase in the downward long wave radiation flux; however, the reduced cloud cover that is associated may lead to a decrease in long wave radiative flux.

Increased mean surface radiation and decreased evaporation (see Fig. 3) cause high temperatures over the continent in the future climate, whereas Atlantic sea surface temperature increases are moderate. The resulting enhanced land-sea temperature contrast increases the dependency of the different surface energy budget terms on the circulation. In particular, the downward long wave radiative and the sensible heat flux are directly affected leading to higher variability, but also

evaporation (higher moisture deficit between atmosphere and the soil) and cloud fields may respond strongly to the enhanced land-sea temperature contrast. We note that, in general, models with the highest land-sea temperature contrast also displayed the largest temperature variability.

5.2 Sensitivity to circulation biases

In Van Ulden et al. (2007) it is shown that the HadAM3H simulation is characterized by a too weak mean westerly flow in summer, but the variability around this mean flow appears realistic. To estimate the potential influence of these deviations in circulation statistics we briefly present results of RACMO2 driven by analyses of the ERA-40 project. The results (period 1961-1990) are shown in Figs. 5, 6, 7 and 8 labeled with R-ERA40. In general, the differences in Δt2m between the two simulations are smaller than one °C. The inter-annual variability in both RACMO2 runs is (very) close to the observations. The differences in the surface fluxes are also not large. It is noted that for mean temperature the results are also similar except for south-eastern part of the domain. In that area, temperatures obtained with ERA-40 boundaries are 1–2°C lower than those obtained with the HadAM3H boundaries. These results suggests that the bias in the circulation statistics in the HadAM3H boundaries is not a critical issue here. But one should be careful not to over-interpret these results since the RACMO2 model has a rather large soil moisture capacity (Van den Hurk et al. 2005) and might therefore be rather insensitive to a mean easterly bias in the circulation.

5.3 Model characteristics

Specific model characteristics are summarized in terms of the relative behavior of the model considered compared to the ensemble mean. These characteristics are inferred mainly from the model results for central Europe (areas GER and SFRA). PROMES and to a lesser degree CLM, HIRHAM and HadRM3H are characterized by relatively large values of ΔSWnet, reflecting a large influence of clouds on radiation. This might be caused by both the amount of clouds simulated and the radiative properties of these clouds. Conversely, in CHRM and too a lesser degree RACMO2 the impact of clouds on radiation appears rather small. HadRM3H, and too a lesser degree HIRHAM, CLM, RegCM, and RCAO are characterized by relatively large negative values of Δevap, which can be attributed to a large sensitivity of the model to soil drying. RACMO2, PROMES and REMO, however, appear rather insensitive to soil drying, but we note that mean evaporation in PROMES is rather low. We note that these model characteristics also appear to be reflected in results of an analysis of daily maximum temperatures in summer (Kjellström et al. 2007).

It is important to note that in the models the above characteristics for evaporation and short wave radiation are not independent. For example, in HadRM3H relatively high evaporation rates and high short-wave radiation during early summer cause a higher sensitivity of the model to soil drying during late summer. On the other extreme, (very) low short wave radiative fluxes and low evaporation rates in PROMES leave the model rather insensitive to soil drying, despite that this model appears to have rather small soil water storage capacity (Van den Hurk et al. 2005). Also, soil drying has an impact on clouds and short wave radiation. A strong drying out of the

soil in southeastern Europe may cause relatively high values of ΔSWnet in central Europe, as appears discernible for the models sensitive to drying for GER in August.

6 Conclusions

The temperature variability of monthly mean temperatures in summer in an ensemble of nine different RCMs driven by HadAM3H-A2 boundaries is studied. The temperature variability in the control simulation of most (but not all) RCMs is significantly overestimated in Central Europe, in some RCMs up to 50–100%, compared to the CRU TS2 2.0 observational data set. Results of a run with re-analysed boundaries of one RCM (RACMO2) suggests that the use of HadAM3H boundaries is not likely to be the major cause for the overestimation of the temperature variability, although it may contribute to some extent.

An analysis of the surface energy budget and its relation with the temperature variability is presented. A reasonable relation between the sum of net short wave radiation, downward long wave radiation, and evaporation, on the one hand, and temperature variability, on the other hand, could be established in the model ensemble (see Fig. 9). For the control integration, there are large differences in how much short wave radiation contributes to the temperature variability, with values of the surface forcing differing a factor five in Germany in France. For evaporation, most RCMs agree in Spain, and Germany, but disagree rather strongly in the intermediate areas, in particular for southern France. The modelled fluxes of evaporation and short wave radiation appear to be the main contributors to the overestimation of the temperature variability.

The temperature variability increases from the control to the future simulation. This increase is particularly large for central Europe (areas GER and SFRA), and smaller for areas in southern Europe (SEU and SPA). In general, the drying out the soil leads to an increased contribution of evaporation to the temperature variability, although there is a considerable spread between the models. The corresponding signal for short wave radiation is not so clear in the model ensemble, although in central Europe on average the effect is positive. In all models, the change in downward long-wave radiation contributes to the increase in temperature variability.

Our results basically reflect that the climate of central Europe is critically dependent on the water and energy budget; they support the notion that the representation of soil moisture control on evaporation (see also e.g. Vidale et al. 2007) and clouds and radiation in regional models are critically determining the climate sensitivity of western Europe in summer. In this respect, this study should not be (primarily) considered as a quality assessment of the models, but merely an evaluation of the uncertainty given present-day, state-of-the-art representations of the water and energy budgets. Given the sensitivity of the climate system in central Europe, the value of using a multi-model ensemble to represent the uncertainty is evident. To reduce the uncertainty comparisons with observations are compulsory.

Acknowledgements The authors would like to thank Olé Christensen and Jens Christensen for their central role in PRUDENCE. Comments by D. Jacob, E. Kjellström, S. Hagemann, R. Jones, F. Giorgi and D. Rowell and two reviewers are acknowledged. The RCM data were obtained with financial support of the EU (Contract EVK2-2001-00156 PRUDENCE).

References

Beniston M, Diaz HF (2004) The 2003 heat wave as an example of summers in a greenhouse climate? Observations and climate model simulations for Basel, Switzerland. Glob Planet Change 44: 73–81

Christensen JH, Christensen OB (2007) A summary of the PRUDENCE model projections of changes in European climate by the end of this century. Clim Change, doi:10.1007/s10584-006-9210-7 (this issue)

Giorgi F, Bi X, Pal J (2004) Means, trends and interannual variability in a regional climate change experiment over Europe. Part I: Present day climate (1961-1990). Clim Dyn 22:733–756

Jacob D, Bärring L, Christensen OB, Christensen JH, de Castro M, Déqué M, Giorgi F, Hagemann S, Hirschi M, Jones R, Kjellström E, Lenderink G, Rockel B, Sánchez E, Schär C, Seneviratne SI, Somot S, van Ulden A, van den Hurk B (2007) An inter-comparison of regional climate models for Europe: Model performance in present-day climate. Clim Change, doi:10.1007/s10584-006-9213-4 (this issue)

Kjellström E, Bärring L, Jacob D, Jones R, Lenderink G, Schär C (2007) Variability in daily maximum and minimum temperatures: Recent and future changes over Europe. Clim Change, doi:10.1007/s10584-006-9220-5 (this issue)

Lenderink G, van Ulden A, van den Hurk B, van Meijgaard E (2006) Summertime inter-annual temperature variability in an ensemble of regional model simulations: analysis of the surface energy budget. Technical report WR-2006-04, Royal Netherlands Meteorological Institute

Luterbacher J, Dietrich D, Xoplaki E, Grosjean M, Wanner H (2004) European seasonal and annual temperature variability, trends and extremes since 1500. Science 303:1499–1503

New M, Hulme M, Jones P (2000) Representing twentieth-century space-time climate variability. Part II: Development of 1901-1996 monthly grids of terrestrial surface climate. J Climate 13:2217–2238

Räisänen J, Hansson U, Ullerstig A, Döscher R, Graham LP, Jones C, Meier HEM, Samuelsson P, Willén U (2004) European climate in the late twenty-first century: regional simulations with two driving global models and two forcing scenarios. Clim Dyn 22:13–31

Schär C, Vidale PL, Lüthi D, Frei C, Häberli C, Liniger MA, Appenzeller C (2004) The role of increasing temperature variability in European summer heatwaves. Nature 427:332–336 doi:10.1038/nature02300

Seneviratne SI, Pal JS, Eltahir EAB, Schär C (2002) Summer dryness in a warmer climate: a process study with a regional climate model. Clim Dyn 20:69–85

Van den Hurk B, Hirschi M, Schär C, Lenderink G, van Meijgaard E, van Ulden A, Rockel B, Hagemann S, Grahan P, Kjellström E, Jones R (2005) Soil control on runoff response to climate change in regional climate model simulations. J Climate 18:3536–3551

Van Ulden A, Lenderink G, van den Hurk B, van Meijgaard E (2007) Circulation statistics in the PRUDENCE ensemble. Clim Change, doi:10.1007/s10584-006-9212-5 (this issue)

Vidale PL, Lüthi D, Frei C, Seneviratne SI, Schär C (2003) Predictability and uncertainty in a regional climate model. J Geophys Res 108(D18):4586, doi:10.1029/2002JD002810

Vidale PL, Lüthi D, Wegmann R, Schär C, (2007) European climate variability in a heterogeneous multi-model ensemble. Clim Change, doi:10.1007/s10584-006-9218-z (this issue)